

Article

Investigation of TiO₂ Nanoparticles Synthesized by Sol-Gel Method for Effectual Photodegradation, Oxidation and Reduction Reaction

Mohamad M. Ahmad ^{1,*}, Shehla Mushtaq ², Hassan S. Al Qahtani ³, A. Sedky ⁴ and Mir Waqas Alam ^{1,*}¹ Department of Physics, College of Science, King Faisal University, P.O. Box 400, Al-Ahsa 31982, Saudi Arabia² School of Natural Sciences, National University of Sciences and Technology, Islamabad 44000, Pakistan; shehla.mushtaq@sns.nust.edu.pk³ EXPEC Advanced Research Centre, Saudi Aramco, Dhahran 31311, Saudi Arabia; Hassan.alqahtani.2@aramco.com⁴ Department of Physics, Faculty of Science, Assiut University, Assiut 71516, Egypt; sedky1@aun.edu.eg

* Correspondence: mmohamad@kfu.edu.sa (M.M.A.); wmir@kfu.edu.sa (M.W.A.)

Abstract: Metal oxide titanium dioxide (TiO₂) nanoparticles were synthesized by using a simple and economical sol-gel method. The prepared nanoparticles were used to evaluate methylene blue dye degradation and as catalysts in the oxidation of benzaldehyde. The crystallite size of the titanium dioxide nanoparticle was 18.3 nm, which was confirmed by X-ray diffraction analysis. The spherical morphology was confirmed by scanning electron microscopy (SEM), and the elemental composition of the nanoparticle was found by energy dispersive X-ray (EDAX) analysis. The anatase form of the nanoparticle was confirmed by the bandgap 3.2 eV, which was measured using UV-DRS analysis. The bond between metal and oxygen was confirmed by the peaks at 485 and 606 cm⁻¹ analyzed by Fourier transform infrared analysis (FTIR). The efficiency of the catalyst in dye degradation was 60.08, 68.38, and 80.89% with respect to 50, 75, and 100 mg catalyst weight. The yield % of benzoic acid was 94%, and the reduction efficiency against 4-nitrophenol was 98.44%.

Keywords: benzaldehyde; degradation; metal oxide; methylene blue; nanoparticle; nitrophenol



Citation: Ahmad, M.M.; Mushtaq, S.; Al Qahtani, H.S.; Sedky, A.; Alam, M.W. Investigation of TiO₂ Nanoparticles Synthesized by Sol-Gel Method for Effectual Photodegradation, Oxidation and Reduction Reaction. *Crystals* **2021**, *11*, 1456. <https://doi.org/10.3390/cryst11121456>

Academic Editor: Yongsheng Han

Received: 7 November 2021

Accepted: 24 November 2021

Published: 25 November 2021

Publisher's Note: MDPI stays neutral with regard to jurisdictional claims in published maps and institutional affiliations.



Copyright: © 2021 by the authors. Licensee MDPI, Basel, Switzerland. This article is an open access article distributed under the terms and conditions of the Creative Commons Attribution (CC BY) license (<https://creativecommons.org/licenses/by/4.0/>).

1. Introduction

In the present era, nanotechnology and nanomaterials play significant roles in many fields, with environmental applications, energy storage devices, and biological applications [1,2].

Nanomaterials possess unique optical, mechanical, and electrical properties due to their size, shape, stability, chemical composition, crystal structure, surface area, etc. Metal oxides such as TiO₂, MoO₃, WO₃, CuO, etc. are less toxic in nature and are used in diverse applications. Among these, TiO₂ is considered a promising candidate for these applications due to its unique properties, such as a wide bandgap. These metal oxide nanoparticles can be synthesized via both top-down and bottom-up approaches. Out of numerous synthesis methods, the sol-gel method, has been verified as a superior route to control the bulk and surface properties of the oxides at low temperature [3–5]. The sol-gel system is an efficient and inexpensive technique used in nanoparticle fabrication. This method yields high crystal oxides by allowing regulation of nanoparticles' size and surface morphology, in addition to phase arrangement in diverse concentration precursors, and it is simple to perform [6].

With increased industrialization and urbanization, water pollution has increased. Due to water pollution, humans are affected by diseases, such as cholera, diarrhea, and hepatitis. Organic dyes are also a major constituent present in polluted water, discharged from the textile, food, and cosmetic industries. Among the discharged organic dyes, methylene blue (MB) is considered one of the most toxic, causing eye irritation, vomiting, nausea, and confusion [7]. Therefore, it is important to discover a suitable material to remove this harmful dye from polluted water [8,9]. Numerous methods can be employed to remove

organic pollutants present in the water, such as adsorption, photodegradation, flocculation, coagulation, and electrocoagulation [10,11]. Of these methods, photocatalytic degradation is an efficient method as the nanocatalyst oxidizes organic compounds into inorganic matter, such as CO_2 and H_2O without any intermediate pollutants [12].

Oxidation of benzaldehyde to benzoic acid is an important process, as benzoic acid is a valuable chemical and is highly used as a precursor in several other molecules. In addition to that benzoic acid is highly used in medicine, food, and chemical industries. For environmental purification, the most familiar oxidation reactions are those that oxidize organic composites [13,14]. Furthermore, the nanostructure is highly utilized as a cocatalyst for H_2O oxidation [15,16]. The heterogeneous catalyst offers an opportunity to degrade organic compounds through either oxidation or reduction reactions. The outcomes show the usefulness of a broad range of materials in the elimination of phenolic compounds from water and wastewater. Nitro groups containing pollutants are of major concern, as they are difficult to reduce due to their toxic behavior. Compounds such as 4-nitro phenol (4-NP) and are toxic but also anthropogenic and inhibitory in nature, so their reduction is an issue of major importance. For instance, 4-nitrophenol is a phenolic compound, constituting one nitro group present on the benzene ring diagonally to the hydroxyl group. Further, 4-NP causes eye irritation and inflammation. It interacts with blood and forms methemoglobin, which results in methemoglobinemia causing cyanosis, confusion, and unconsciousness. When ingested, it causes abdominal pain and vomiting. Moreover, 4-NP and its byproducts are used for the synthesis of herbicides, insecticides, and pesticides that threaten the environment as well as human beings [17]. Nitrophenols are among the main organic pollutants in wastewater produced from agricultural and industrial sources. Therefore, the increase in an efficient and environmentally friendly process to eliminate them from water is highly significant [18].

Metal oxide nanoparticles, such as iron oxide (Fe_3O_4), manganese oxide (Mn_2O_3), copper oxide (CuO), nickel oxide (NiO), zinc oxide (ZnO), etc., act as photocatalysts, which play a significant role in the removal of MB from polluted water [19–21]. For photocatalysis applications, titanium is highly used, known as the ninth most abundant element present in Earth's crust. Since the photoinduced and electrochemically facilitated degradation of HO was reported by Fujishima and Honda in the 1970s, titanium metal has been considered an attractive compound, which possesses several promising applications in photocatalysis [22,23]. Titanium dioxide (TiO_2) exists in three forms—anatase, rutile, and brookite. It also exists in mixed phases of rutile–anatase, anatase–brookite, and anatase–rutile–brookite. In a mixed phase, the flow of electrons from the anatase to a lower-energy rutile-trapping site could limit charge carrier recombination and efficiently establish catalytic hot spots. Only a few brookite reports have been published due to low photocatalytic activity [24].

Both anatase and rutile have tetragonal structures, and brookite has an orthorhombic structure. Rutile is the most stable, while anatase and brookite are metastable at ambient temperature [22,25]. In comparison with rutile, anatase exhibits higher transparency in the near-ultraviolet spectrum. Many researchers examine the TiO_2 nanoparticle (TiO_2 NP) due to its less toxic nature, ease of handling, economical cost, and good resistance to chemical and photochemical erosion [26]. These properties lead TiO_2 NPs to play important roles in sensors, solar cells, environmental remediation, self-cleaning, and hydrogen gas evolution. The mobility of the electron is very high in anatase TiO_2 , and therefore, it is used as a photoanode material in dye-sensitized solar cells [27]. A recent statistical analysis showed that the research publications on the photocatalysis of TiO_2 have reached 10,000 each year since 2000. This proves that this material has broad applications due to its excellent properties. Due to the surface-to-volume ratio of nanostructured TiO_2 , the rate of the photocatalytic process is highly increased, compared with the bulk [28,29]. Owing to the redox properties of TiO_2 , it is highly used in both oxidation and reduction reactions, such as oxidation of organic contaminants and reduction of metals and organic pollutants [30,31]. Due to the faster recombination process of the photogenerated electron–electron, pure TiO_2 comprises restrained photocatalytic activities, and during the process, unproductive

energies are released either in the form of photon production or heat [32,33]. In this study, the TiO₂ NP was synthesized by the sol-gel method. The synthesized nanoparticle was analyzed by UV-DRS spectrophotometry, FTIR spectrophotometry, XRD, SEM, and EDX. The efficiency of the material was verified in terms of MB dye degradation, conversion of benzaldehyde to benzoic acid by the oxidation process, and 4-nitrophenol to 4-aminophenol by the reduction process.

2. Experiment

2.1. Materials

Titanium tetra isopropoxide Ti[(OCH)(CH₃)₂]₄ (97% purity) and glacial acetic acid (CH₃COOH) (100% purity) were used as precursor materials in TiO₂ nanoparticles synthesis. Benzaldehyde (99% purity), hydrogen peroxide (30% purity), and dimethylformamide (99.5% purity) were used in the oxidation of benzaldehyde to benzoic acid. In addition, 4-Nitrophenol (99.5% purity) and sodium borohydride (NaBH₄) (96% purity) were used in the reduction process. Methylene blue dye was chosen as a pollutant for the degradation process. The materials used for synthesis and application were purchased from Merck. Double distilled water was used as a solvent during the synthesis and application process.

2.2. Synthesis of TiO₂ Nanoparticles

Titanium tetra isopropoxide, glacial acetic acid, and double distilled water were used to synthesize TiO₂ nanoparticles as a starting material. First, 15 mL of acetic acid was blended with 150 mL of double-distilled water and stirred continuously for 30 min under 0 °C, keeping the titania solution beaker in an ice-containing bowl. Then, 5 mL of titanium tetra isopropoxide was added drop by drop and stirred vigorously for 5 h. To obtain a clear solution, the above reaction mixture was ultrasonicated for 30 min, and it was kept in the dark for up to 24 h without disturbance for the nucleation process. Then, the solution was kept in a hot air oven at 80 °C for 10 h to obtain a gel. The obtained gel was kept in an oven at 100 °C until completely dry. The dried material was finely powdered by using a mortar and pestle and calcinated at 600 °C for 5 h to obtain the white color TiO₂ nanoparticles.

2.3. Characterization

The crystallite size, plane, and phase of the TiO₂ NPs were assessed using X-ray diffraction analysis performed by an XRD spectrometer (Rigaku-Tokyo, Japan). Cu K α was used to perform the analysis with $\lambda = 1.540 \text{ \AA}$, 40 kV, and 30 mA, and D/teX Ultra was used as a detector. The analysis was recorded in the range of 10–80° with the scan rate of 10°/min. The crystallite size was measured by the Debye–Scherrer equation. The average particle size and morphology were observed by scanning electron microscopy using Bruker. The average particle size of the nanoparticle was calculated using ImageJ software. The elemental composition, such as atomic and weight percentage, was identified by EDX analysis. The functional group present in the nanoparticle was confirmed by FTIR analysis by a Jasco spectrophotometer, and KBr was used as the standard for the preparation of the pellet. The analysis was recorded in the range from 4000 to 400 cm⁻¹. The optical property of the nanoparticle was analyzed by a UV-2600 ISR 2600 PLUS spectrophotometer, Shimadzu, Japan. The UV-DRS analysis was recorded in the range of 200–800 nm.

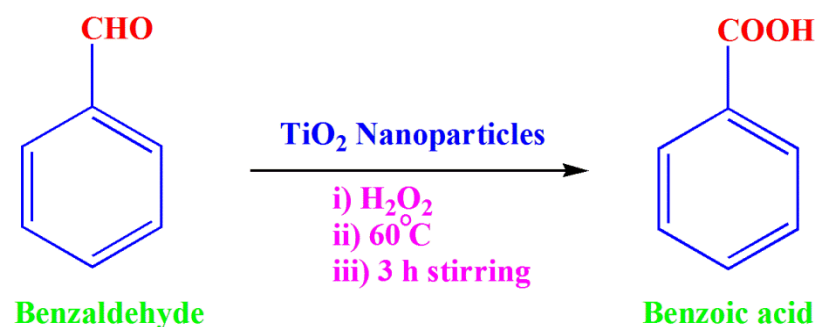
2.4. Photocatalytic Degradation Study

The photocatalytic degradation of MB was performed by using TiO₂ NPs as an effective catalyst. The degradation study was carried out in a batch reactor system with an open rectangular tray made of borosilicate glass. The tray consisted of 250 mL of a known concentration (100 μM) of dye solution with a known weight of the catalyst. The pH of the solution was maintained at 7 ± 0.1 . Then, it was stirred with medium rotation per minute (rpm) for 30 min in the dark to attain adsorption–desorption equilibrium. The absorbance of the dye solution was measured at 665 nm using UV-Vis spectrophotometry before the degradation process. Then, the degradation study was performed under direct sunlight

irradiation. The intensity of the sunlight irradiation was measured frequently using a flux meter, and it was observed to be in the range of 820–830 lx. The degraded solution was collected at particular time intervals, and the collected solution underwent an absorbance study to calculate the efficiency of the catalyst.

2.5. Oxidation of Benzaldehyde to Benzoic Acid

The oxidation reaction of benzaldehyde to benzoic acid was performed at room temperature using TiO₂ NPs as an effective catalyst. For the oxidation study, a 5 mL benzaldehyde solution was taken as a precursor material, and 10 mg of catalyst was added to the precursor. This reaction mixture was continuously stirred for 3 h at 60 ± 5 °C. To this, 12.5 mL of hydrogen peroxide was added drop wise, which acted as an oxidizing agent. Then, the above reaction mixture was stirred for 3 h. After completion of the reaction, the reaction mixture was cooled, filtered, washed, and dried. The obtained material was recrystallized using dimethylformamide. The recrystallized product was taken as a final product, and it was weighed accurately. Scheme 1 shows the oxidation of benzaldehyde to benzoic acid in the presence of TiO₂ NPs as a catalyst.



Scheme 1. Oxidation of benzaldehyde to benzoic acid.

2.6. Reduction of 4-Nitrophenol to 4-Aminophenol

The TiO₂ nanoparticle was used as a catalyst in the conversion of 4-Nitrophenol to 4-Aminophenol (reduction reaction) with NaBH₄ as a reducing agent, and the reaction was achieved at room temperature. In total, 5 mmol of 4-nitrophenol was dissolved using double distilled water in a 100 mL standard flask. At the same time, 0.001 mmol of NaBH₄ was dissolved in 4 mL of distilled water. Next, 20 mL of prepared 4-nitrophenol solution and sodium borohydride solution were added to a 100 mL beaker. Both the solutions were stirred for 15 min constantly. To the above reaction mixture, 0.5 mg of catalyst was added, and using the magnetic stirrer, the solution was stirred for 5 min. The optical density values were recorded using UV-Vis spectrophotometry for every 1-minute time interval for the above reaction mixture.

3. Results and Discussion

3.1. XRD Analysis

Figure 1 shows the XRD pattern of TiO₂ NPs. From the XRD analysis (Rigaku, Tokyo Japan), the 2θ values were observed at 25.33, 36.01, 37.90, 48.06, 53.96, 55.06, 62.70, 69.01, and 70.41° with respect to the planes (101), (103), (004), (200), (105), (211), (204), (116), and (220). The diffraction peaks showed that the formed nanoparticles exhibited anatase phase, which was confirmed by the JCPDS card No. 84-1285. The average crystalline size of the TiO₂ nanoparticles was calculated using Debye–Scherrer Equation (1) and was 10.88 nm.

$$D = \frac{K\lambda}{\beta \cos\theta} \quad (1)$$

where K is constant, λ = wavelength of X-rays, and β Full width at half maximum (FWHM).

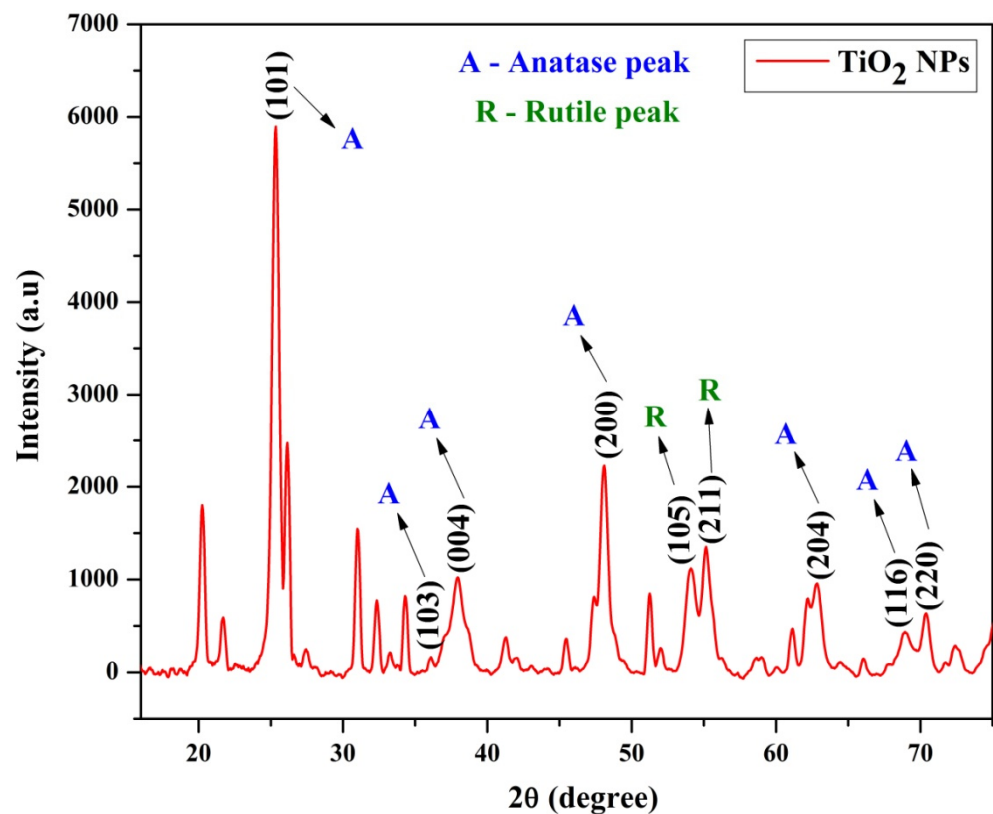


Figure 1. XRD analysis of TiO₂ nanoparticles.

The (101) plane of anatase TiO₂ was represented by the strongest diffraction peak situated at 25.33°. The peaks other than 53.96 and 55.06° are accountable to the anatase structure, and 53.96 and 55.06° are responsible for the rutile structure. This suggests that the major crystal phase present in the TiO₂ nanoparticles was anatase, and some rutile phases were present in the synthesized sample with minimum quantity. From the XRD, the broad peaks displayed that the particles were nanometer size. These results are in good agreement with the previous investigation by Liu et al. [34]. Dubey et al. synthesized TiO₂ NPs, which displayed anatase phase with main diffraction peaks at 25 and 48, with no impurities present in the sample. This suggested that the TiO₂ NPs had a tetragonal anatase structure with trigonal planar and octahedral geometry [35].

3.2. SEM–EDX Analysis

The morphology of the TiO₂ NPs was identified as spherical and rod with slight agglomeration. The average particle size of the TiO₂ NPs was 121 nm. Figure 2a,b show the SEM analysis (Bruker, Karlsruhe, Germany) of TiO₂ nanoparticles at 1 μm and 500 nm, respectively. Agglomeration of nanoparticles is due to the adhesion of particles to each other by weak forces leading to (sub) micron-sized entities and high surface energy. Depending on the synthesis conditions such as environmental factors, temperature, and surface chemistry, the nanoparticles tend to form soft or hard agglomerates. Figure 2c shows the EDX analysis (Bruker, Karlsruhe, Germany) of the TiO₂ nanoparticles. Similarly, irregular and spherical TiO₂ NPs with aggregation were obtained by the sol-gel method [36]. Chu et al. reported that TiO₂ NPs displayed regular particles with ammonium fluoride rather than water, and the as-prepared particles were nanowire in morphology. The material with water revealed an irregular shape, and the nanoparticles showed mixed morphology such as rod, sphere, and ellipsoid. According to Chu's report, ammonium fluoride acted as a shape-controlling agent, which directed the decomposition of nanowires into regular particles [37]. The elemental atomic percentage of the Ti, O, and C were 26.4%, 69.48%, and

4.12%, respectively. The weight percentage of the Ti, O, and C were 44.35%, 41.65%, and 14%, respectively, which was determined through EDX analysis.

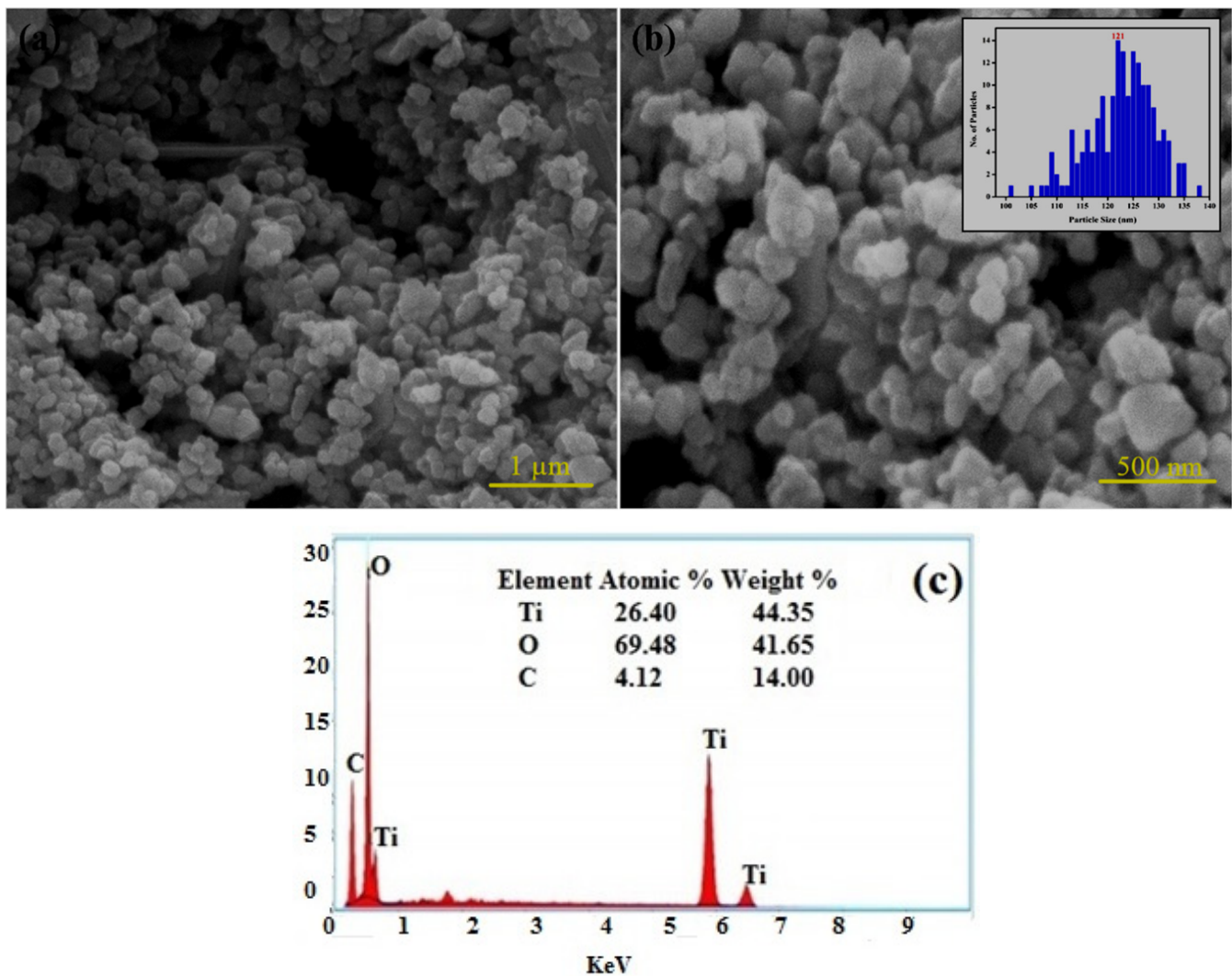


Figure 2. SEM–EDX analysis of TiO₂ nanoparticles: (a) SEM image at 1 μm; (b) 500 nm; (c) EDX analysis.

3.3. UV–DRS Analysis

The absorption maximum of the TiO₂ NP was 386 nm, determined by UV–DRS spectrophotometry (ISR 2600 Plus, Shimadzu, Tokyo, Japan). By using the Tauc plot (Equation (2)), the bandgap energy of the synthesized TiO₂ NP was calculated as 3.2 eV, and it was an indirect bandgap [38]. Figure 3a shows the UV–DRS spectrophotometry and b the Tauc plot. In our study, the undoped TiO₂ NP exhibited absorption at less than 387 nm, as compared with the previous study of iron, silver, cobalt doped titanium oxide nanoparticles, due to the inherent bandgap of anatase TiO₂, and it was accredited to the band-to-band transition reported by Babji et al. [39]. The decreasing particle size increased the bandgap of the material, and the absorption edge was transferred to higher energy, which was blueshift. In this regard, the bandgap of the semiconductor material was size dependent [40].

$$\alpha h\nu = E_d(h\nu - E_g)^{1/2} \quad (2)$$

where α = optical absorption coefficient, $h\nu$ = photon energy, E_g = direct band gap, and E_d = constant.

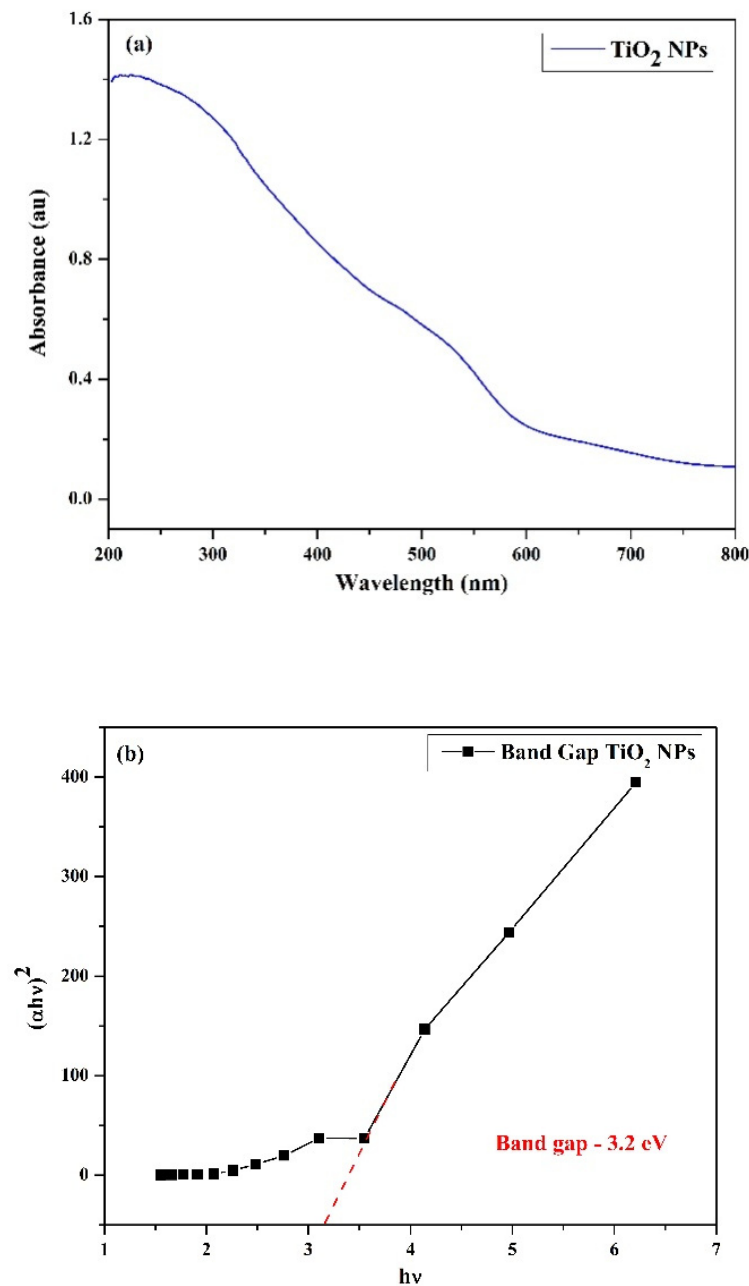


Figure 3. (a) UV-DRS spectrophotometric analysis and (b) Tauc plot of TiO₂ nanoparticles.

3.4. FTIR Analysis

Figure 4 shows the FTIR analysis (Jasco, Tokyo, Japan) of TiO₂ NPs. The Ti-O bond formation was confirmed by the peak appearing at 485 and 606 cm⁻¹. This suggests that the formed nanoparticle was anatase in structure [41,42]. The band that appeared at 1632 cm⁻¹ was attributed to the absorption of water molecules, present in the atmosphere, by nanoparticles during the analysis. The hydroxyl group present in the synthesized TiO₂ NP was confirmed by the band appearing at 3431 cm⁻¹. From the analysis, the peak that appeared at 1632 and 3431 cm⁻¹ indicates the hydroxyl group was present on the surface of the TiO₂ nanoparticles. The band appearing at 2919 cm⁻¹ was attributed to the existence of the asymmetric C-H group in the nanoparticles [43]. According to Samira et al., the absence of a band around 2900 cm⁻¹ is due to the complete elimination of organic molecules at high calcination temperatures [44]. The organic molecules present in the nanoparticles were removed by calcination.

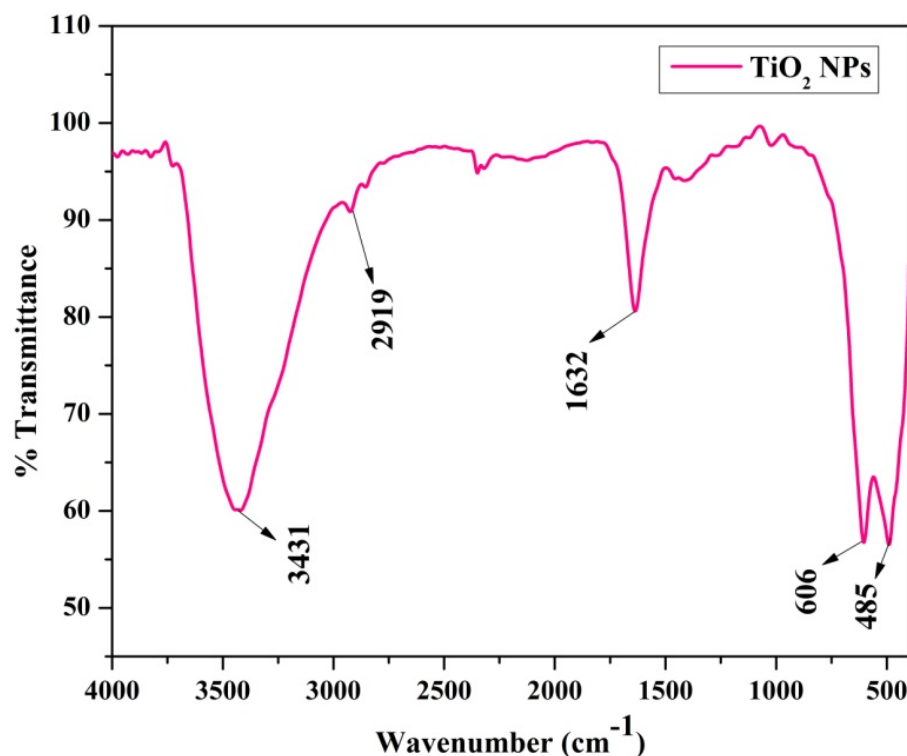


Figure 4. FTIR spectrophotometric analysis of TiO₂ nanoparticles.

3.5. Photocatalytic Degradation of the Dye Solution

Effect of Catalyst Weight

Metal oxides, such as CdS, Mn₂O₃, ZnO, ZrO₂, Fe₃O₄, etc., act as better catalysts due to their remarkable bandgap and high photocatalytic activity. In this study, TiO₂ NP was used as an efficient catalyst in the degradation of MB dye solution of known concentration (100 μM) with different catalyst weights of 50 mg, 75 mg, and 100 mg at pH 7 ± 0.1. The efficiency percentage was calculated using Equation (3). The absorption spectrum of the degraded solution steadily decreased as the reaction time increased, which may be due to the degradation of the chromophore present in MB. The efficiency percentage of the degradation of MB dye solution using TiO₂ NP was 60.08, 68.38, and 80.89%, with respect to the catalyst weights 50, 75, and 100 mg. The photodegradation of MB dye by TiO₂ NP is shown in Figure S1 (in Supplementary Materials). Figure 5a shows the plot of time vs. absorbance, Figure 5b shows the plot of time vs. % degradation, Figure 5c shows the linear regression graph with respect to time vs. ln (c₀/c_t), and Figure 5d shows the degradation % with respect to the number of cycles. The highest response can be clearly seen at 100 mg with the first run. The correlation coefficient (R²) of the degradation of MB dye with different catalyst weights 50, 75, and 100 mg was 0.7945, 0.9550, and 0.9598, respectively. The rate constant (k) for degradation of the dye solution with different catalyst weights 50, 75, and 100 mg was 15.3 × 10⁻³, 19.1 × 10⁻³, and 27.5 × 10⁻³ min⁻¹, respectively. The photocatalytic degradation reaction of MB increased with an increase in catalyst weight, due to the increased number of active sites present on the surface of the catalyst. If the active site of the catalyst is higher, it increases the number of photons adsorbed, which allows a higher number of dye molecules to be mineralized. The absorbance and % degradation of the dye with respect to time in presence of different weight catalysts are shown in Supplementary Data (Table S1).

$$\text{Degradation \%} = (A_0 - A_t/A_0) \times 100 \quad (3)$$

where A₀—absorbance at the initial time, and A_t—absorbance at different time intervals.

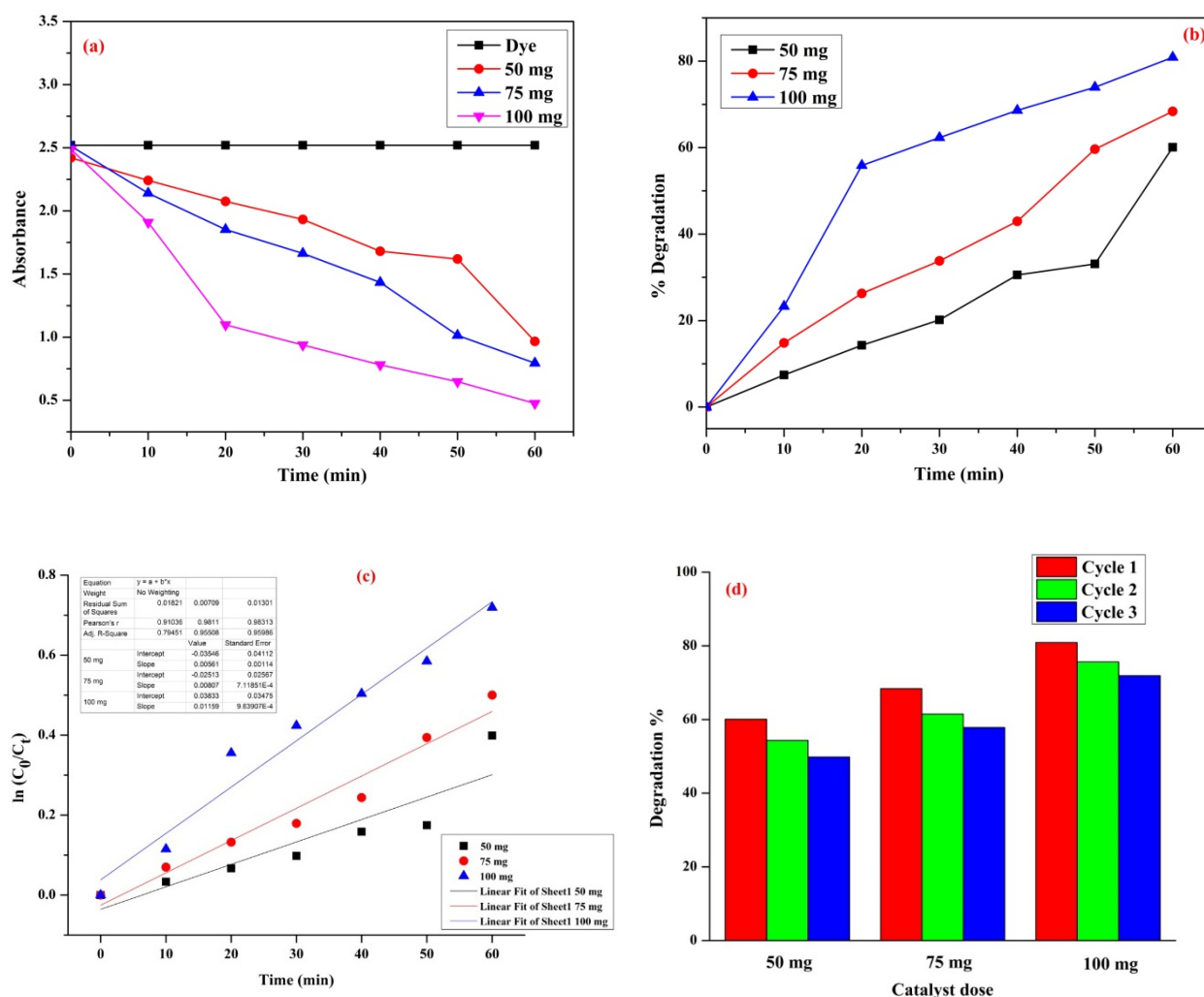


Figure 5. (a) Plot of time vs. absorbance, (b) plot of time vs. % Degradation, (c) linear regression graph of MB degradation using different catalyst weights, and (d) plot for number of cycles using different catalyst doses vs. % degradation.

The photocatalytic activity of TiO₂ NPs was enhanced by the spherical morphology and small crystallite size. The TiO₂ hollow nanofiber showed higher photocatalytic efficiency at 0.75 g/L and moderate at 1.0 g/L, as reported by Jafri et al. [45]. In this degradation process, the nanoparticle had higher active sites at the optimum weight of the catalyst, and there was a gradual decrease in active sites of the nanoparticle as the weight of the catalyst exceeded the optimum weight. This may be caused by the agglomeration of the photocatalyst, which led to a decrease in the precise surface area of the nanoparticle, and owing to the screening effect of a large amount of catalyst, the number of photons received by the active site was decreased [46,47]. According to Muthee et al., the mixed anatase–rutile phase acts as a highly active photocatalyst [48]. The recycling and reusability of the catalyst are important in commercial uses. After the degradation reaction, the catalyst was collected from the dye solution and washed with double distilled water several times, and dried in an oven at 80 °C. The collected catalyst was further used for a reusability study. After two runs, the efficiency of the catalyst decreased, as shown in Supplementary Data (Table S2). The decrease in the photocatalysis activity could be attributed to the following: (1) Material losses might occur in the revival step (washing and drying), which would lead to a lower quantity in the successive cycle, thereby decreasing the surface catalytic activity and degrading the performance; (2) the properties of nanoparticles such as aggregation (this effect can reduce the effective surface area and decrease the number of active sites) might change during the three cycles; (3) the adsorptive catalytic surface activity of the catalyst gradually decreased because of the obstruction of the pores and the active sites.

The related degradation reaction of MB using nanoparticles as an efficient catalyst is shown in Table 1 [49–52]. Sarigul et al. synthesized a hybrid amino acid–TiO₂ nanoparticle for photocatalytic activity and compared its efficiency with commercial TiO₂ (P25). The amino acid with TiO₂ nanoparticle increased the photocatalytic activity against MB degradation under visible light, compared with the commercial P25. This is because the hybrid materials are more stable against both degradation and leaching. Considering the commercial TiO₂, which is P25 (Degussa/Evonik/Nippon Aerosol), a highly used commercial photocatalyst, the degradation time for P25 is 240 min, while our results showed a degradation time of 60 at an even higher concentration [53].

Table 1. Degradation reaction of MB using nanoparticles as an efficient catalyst.

S. No	Catalyst	Pollutant	Reduction %	Reference
1	α -Fe ₂ O ₃	MB	95%	49
		Methyl orange	94%	
		Bromo green	94%	
		Methyl red	76%	
2	Fe ₂ O ₃ /Mn ₂ O ₃			MB
3	NiFe ₂ O ₄	MB	89%	51
		Methyl orange	92%	
		Bromo green	93%	
		Methyl red	78%	
4	Fe ₃ O ₄ /TiO ₂	MB	97%	52
5	TiO ₂	MB		Present work
		50 mg catalyst	60.08%	
		75 mg catalyst	68.38%	
		100 mg catalyst	80.89%	
		4-nitrophenol	98.44%	
	0.5 mg catalyst			

3.6. Oxidation of Benzaldehyde to Benzoic Acid

The oxidation of benzaldehyde to benzoic acid was completed by using TiO₂ NPs as a catalyst. Figure 6a,b show the FTIR spectrum of the oxidation of benzaldehyde to benzoic acid without and with the catalyst. We performed the conversion of benzaldehyde to benzoic acid using H₂O₂ in the presence of the catalyst, and the same reaction was carried out without the catalyst using H₂O₂. The characteristic peak appearing at 1696 cm⁻¹ was attributed to the existence of the C=O stretching vibration. A peak value was observed at 2863 cm⁻¹ with respect to the –COOH group present in the product, which confirmed the aldehyde converted to acid. The presence of the C=C aromatic stretching vibration was confirmed by the peak observed at 1428 cm⁻¹. The aromatic C-H group was present in the product, as confirmed with the peaks at 684 and 531 cm⁻¹. A peak appeared at 925 cm⁻¹ with respect to the presence of the O-H bending vibration in the benzoic acid, and a peak appeared at 1299 cm⁻¹ corresponding to the C-O stretching vibration. The characteristic peak that appeared at 1695 cm⁻¹ was attributed to the existence of C=O stretching vibration. The peak value observed at 2836 cm⁻¹ with respect to the –COOH group present in the product confirms the aldehyde converted to acid. The presence of C=C aromatic stretching vibration was confirmed by the peak observed at 1430 cm⁻¹. The aromatic C-H group was present in the product was confirmed with the peak 683 and 529 cm⁻¹. The peak appearing at 927 cm⁻¹ with respect to the presence of O-H bending vibration in the benzoic acid, together with the peak appearing at 1291 cm⁻¹, corresponds to C-O stretching vibration. The time taken for conversion of benzaldehyde to benzoic acid without and with a catalyst was nine hours and six hours, respectively. From this, we confirmed that the addition of the catalyst increased the rate of the reaction. The yield of benzoic acid was measured as 3.18 g. The yield % was calculated by following Equation (4).

$$\text{Yield (\%)} = (\text{Actual weight}/\text{Theoretical weight}) \times 100 \quad (4)$$

The mechanism of the oxidation reaction of benzaldehyde to benzoic acid with hydrogen peroxide as an oxidizing agent and TiO₂ NPs as a catalyst is shown in Figure 7. The H₂O₂ was activated on the surface of the catalyst, which occurred through the reaction between the H₂O₂ and –OH group present in the catalyst. This reaction led to the formation of TiO₂-OOH peroxy surface species. Then, the O-O bond was polarized in the species, which led the nucleophilic aldehyde to be attacked by the hydroxyl group and formed benzoic acid as a major product [54].

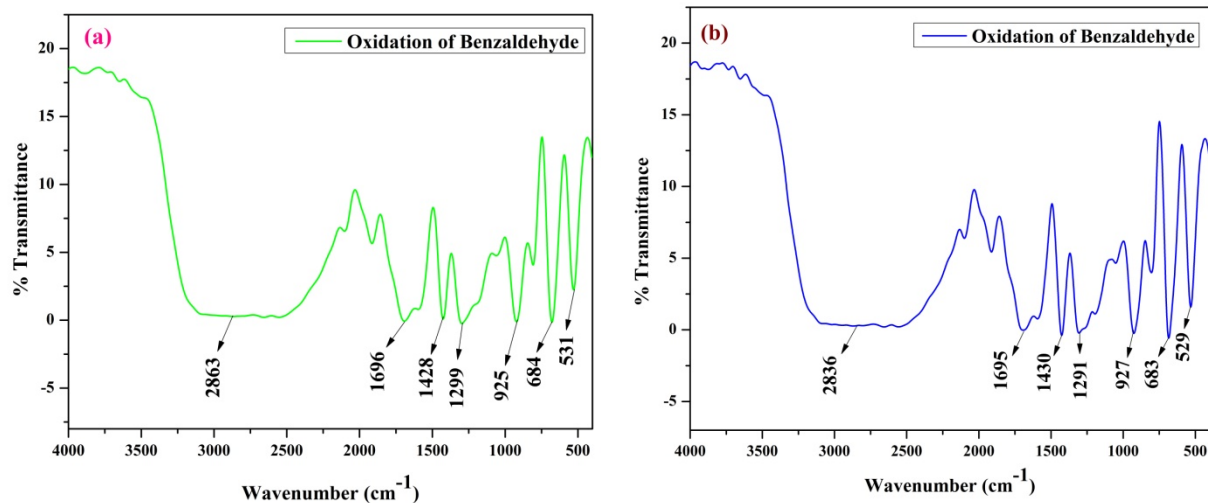


Figure 6. FTIR analysis of the oxidation of benzaldehyde to benzoic acid by TiO₂ nanoparticles: (a) without catalyst and (b) with catalyst.

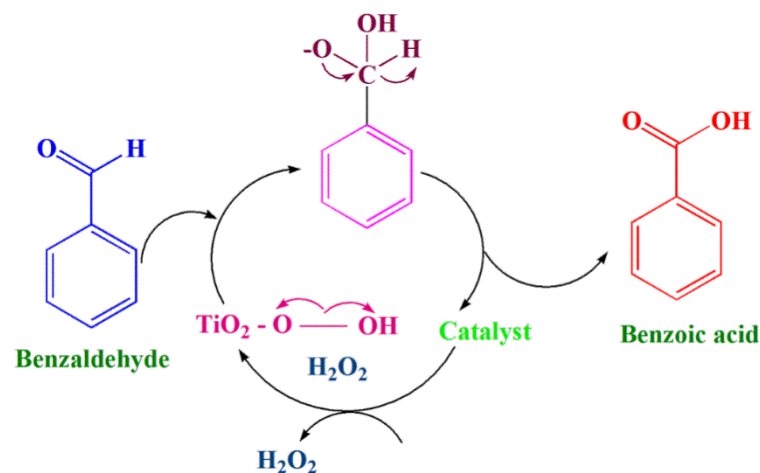


Figure 7. Mechanism of oxidation of benzaldehyde to benzoic acid.

3.7. Reduction of 4-Nitrophenol to 4-Aminophenol

The catalytic efficiency of TiO₂ nanoparticles was studied for the reduction of 4-nitrophenol as a pollutant. In this reduction process, 4-nitrophenol was reduced to 4-aminophenol, and this process was carried out at room temperature. During the process, 4-nitrophenol was changed to phenolate ion as an intermediate, and finally, the intermediate was changed to 4-aminophenol [55]. Figure 8 shows the mechanism of conversion of 4-nitrophenol to 4-aminophenol by the reduction process. The conversion reaction was completed within 20 min, and the absorption was recorded for every 1 minute during the reduction process. A sharp peak with high intensity around 400 nm was observed, which can be accredited to 4-nitrophenol at 0 min, and a broad peak was observed at 300 and 230 nm, which can be

accredited to 4-aminophenol at 20 min. The TiO₂ nanoparticles showed a reduction efficiency of up to 98.44% at the nine-minute interval, and the R² value was 0.9492. Figure 9a shows the plot of Time vs. % Reduction, while Figure 9b shows the linear regression coefficient. Table 2 shows the absorbance and % Reduction with respect to time for 4-nitrophenol reduction.

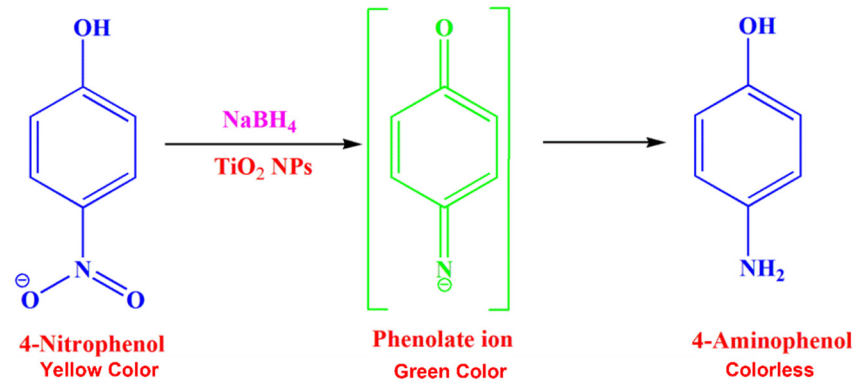


Figure 8. Mechanism of reduction of 4-nitrophenol to 4-aminophenol.

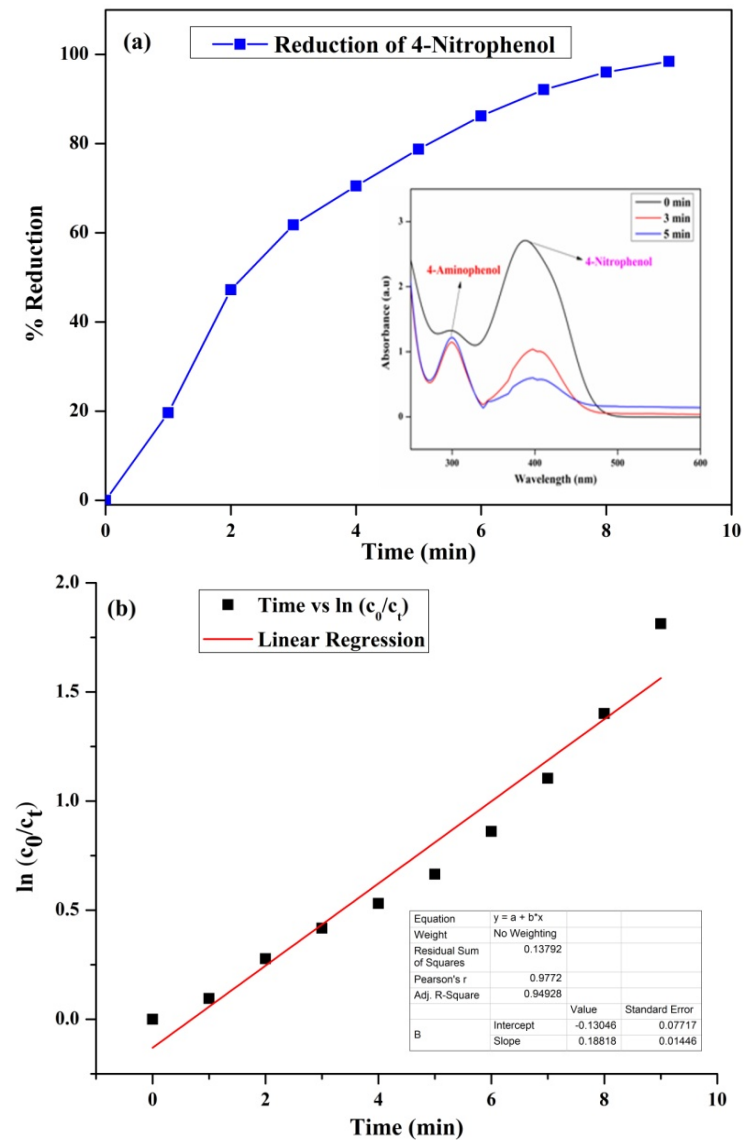


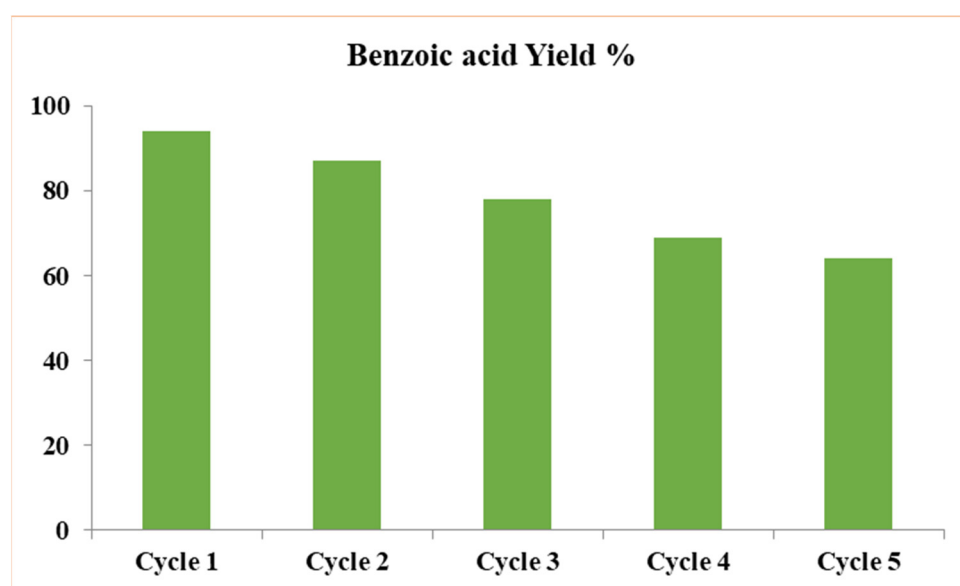
Figure 9. (a) plot of time vs. % reduction and (b) time vs. $\ln(c_0/c_t)$ and linear regression.

Table 2. Absorbance and % reduction with respect to time for 4-nitrophenol reduction.

S. No	Time (min)	Absorbance	% Reduction	ln (c ₀ /c _t)
1	0	2.7234	0	0
2	1	2.1887	19.63	0.0949
3	2	1.4367	47.24	0.2776
4	3	1.0410	61.77	0.4176
5	4	0.8030	70.51	0.5304
6	5	0.5890	78.77	0.6650
7	6	0.3753	86.21	0.8607
8	7	0.2143	92.13	1.1041
9	8	0.1082	96.02	1.4009
10	9	0.0423	98.44	1.8124

3.8. Reusability Study

The reusability of the catalyst is important in industrial aspects. After the completion of the reaction, the catalyst was separated using a separating funnel. The separated catalyst was further washed with double distilled water several times to remove the product and impurities and dried at 80 °C till completely dry. Then, the separated TiO₂ NP was further used for oxidation reaction to verify the reusability of the catalyst, and the same reaction was carried out. The efficiency of the catalyst decreased during five runs, 94, 87, 78, 69, and 64% for benzaldehyde oxidation. Figure 10 shows the yield % of benzoic acid in different cycles. With each cycle, the % yield decreased due to the leaching of the nanoparticle during the washing and drying after every cycle. Therefore, for the first cycle, the efficiency was 94%, and then with each cycle, it decreased until 64% efficiency was achieved in the fifth cycle.

**Figure 10.** Yield % of benzoic acid in different cycles.

4. Conclusions

The anatase TiO₂ NPs were successfully synthesized by a simple sol-gel method. From XRD analysis, the formed nanoparticle showed the anatase structure confirmed with JCPDS card No. 84-1285. The crystallite size of the synthesized nanoparticle was 18.3 nm with spherical morphology. The bandgap (3.2 eV) revealed that the formed nanoparticle was in anatase form. The bond formation between metal and oxide was confirmed by FTIR analysis. The efficiency of degrading the dye solution decreased with the increased use of the catalyst in the reusability study. The yield percentage of conversion of benzaldehyde to benzoic acid also decreased with the increased number of cycles for the same reaction. In the reduction process, 98.44% of 4-nitrophenol was converted to 4-aminophenol. Hence,

it was shown that the TiO₂ NPs were efficient catalysts in the degradation of methylene blue, the oxidation of benzaldehyde, and the reduction of 4-nitrophenol.

Supplementary Materials: The following are available online at <https://www.mdpi.com/article/10.3390/cryst11121456/s1>, Figure S1: Photodegradation of methylene blue dye by TiO₂ nanoparticles for 50 mg, 75 mg and 100 mg; Figure S2: Mechanism of oxidation of benzaldehyde to benzoic acid; Table S1: Absorbance and % degradation of dye with respect to time in presence of different catalyst weight; Table S2: Reusability study of photocatalyst.

Author Contributions: Conceptualization, M.W.A. and M.M.A.; methodology, M.M.A., S.M., and M.W.A.; validation, M.M.A., and M.W.A.; formal analysis, M.M.A., H.S.A.Q., and M.W.A.; investigation, M.M.A., S.M., H.S.A.Q., and M.W.A.; resources, M.M.A., A.S., and M.W.A.; data curation, S.M., H.S.A.Q.; writing—original draft preparation, M.M.A., S.M., H.S.A.Q., A.S., and M.W.A.; writing—review and editing, M.M.A., S.M., H.S.A.Q., A.S., and M.W.A.; visualization, M.M.A., A.S.; supervision, M.M.A., A.S.; project administration, M.M.A., A.S., and M.W.A.; funding acquisition, M.M.A., A.S., and M.W.A. All authors have read and agreed to the published version of the manuscript.

Funding: The authors acknowledge the Deanship of Scientific Research at King Faisal University for financial support under the DSR Annual Project (Grant No. 130153).

Institutional Review Board Statement: Not applicable.

Informed Consent Statement: Not applicable.

Data Availability Statement: Not applicable.

Conflicts of Interest: The authors declare no conflict of interest.

References

1. Lavacchi, A.; Bellini, M.; Berretti, E.; Chen, Y.; Marchionni, A.; Miller, H.A.; Vizza, F. Titanium dioxide nanomaterials in electrocatalysis for energy. *Curr. Opin. Electrochem.* **2021**, *28*, 100720. [CrossRef]
2. Mesgari, M.; Aalami, A.H.; Sahebkar, A. Antimicrobial activities of chi-tosan/titanium dioxide composites as a biological nanolayer for food preservation: A review. *Int. J. Biol. Macromol.* **2021**, *176*, 530–539. [CrossRef]
3. Manikandan, V.; Elancheran, R.; Revathi, P.; Vanitha, U.; Suganya, P.; Krishnasamy, K. Synthesis, characterization, photocatalytic and electrochemical studies of reduced graphene oxide doped nickel oxide nanocomposites. *Asian J. Chem.* **2021**, *33*, 411–422. [CrossRef]
4. Thirugnanasambandham, K.; Sivakumar, V. Modeling and optimization of treatment of milk industry wastewater using chitosan-zinc oxide nanocomposite. *Desalination Water Treat.* **2015**, *57*, 18630–18638. [CrossRef]
5. Avinash, B.; Ravikumar, C.R.; Kumar, M.R.A.; Santosh, M.S.; Pratapkumar, C.; Nagaswarupa, H.P.; Murthy, H.C.A.; Deshmukh, V.V.; Bhatt, A.S.; Jahagirdar, A.A.; et al. NiO bio-composite materials: Photocatalytic, electrochemical and supercapacitor applications. *Appl. Surf. Sci. Adv.* **2021**, *3*, 100049. [CrossRef]
6. Abel, S.; Jule, L.T.; Belay, F.; Shanmugam, R.; Dwarampudi, L.P.; Nagaprasad, N.; Krishnaraj, R. Application of Titanium Dioxide Nanoparticles Synthesized by Sol-Gel Methods in Wastewater Treatment. *J. Nanomater.* **2021**, *2021*, 3039761. [CrossRef]
7. Rafatullah, M.; Sulaiman, O.; Hashim, R.; Ahmad, A. Adsorption of methylene blue on low-cost adsorbents: A review. *J. Hazard. Mater.* **2010**, *177*, 70–80. [CrossRef]
8. Derakhshan, Z.; Baghapour, M.A.; Ranjbar, M.; Faramarzian, M. Adsorption of Methylene Blue Dye from Aqueous Solutions by Modified Pumice Stone: Kinetics and Equilibrium Studies. *Health Scope* **2013**, *2*, 136–144. [CrossRef]
9. Dutta, K.; Mukhopadhyay, S.; Bhattacharjee, S.; Chaudhuri, B. Chemical oxidation of methylene blue using a Fenton-like re-action. *J. Hazard. Mater.* **2001**, *84*, 57–71. [CrossRef]
10. Habib, N.R.; Taddesse, A.M.; Temesgen, A. Synthesis, characterization and photocatalytic activity of Mn₂O₃/Al₂O₃/Fe₂O₃ nanocomposite for degradation of malachite green. *Bull. Chem. Soc. Ethiop.* **2018**, *32*, 101–109. [CrossRef]
11. Ochiai, T.; Fujishima, A. Photoelectrochemical properties of TiO₂ photocatalyst and its applications for environmental purification. *J. Photochem. Photobiol. C Photochem. Rev.* **2012**, *13*, 247–262. [CrossRef]
12. Wang, Y.F.; Tao, J.J.; Wang, X.Z.; Wang, Z.; Zhang, M.; Gang, H.; Sun, Z.Q. A unique Cu₂O/TiO₂ nanocomposite with enhanced photocatalytic performance under visible light irradiation. *Ceram. Int.* **2017**, *43*, 4866–4872. [CrossRef]
13. Chen, C.; Ma, W.; Zhao, J. Semiconductor-mediated photodegradation of pollutants under visible-light irradiation. *Chem. Soc. Rev.* **2010**, *39*, 4206–4219. [CrossRef]
14. Pan, C.; Zhu, Y. New Type of BiPO₄ Oxy-Acid Salt Photocatalyst with High Photocatalytic Activity on Degradation of Dye. *Environ. Sci. Technol.* **2010**, *44*, 5570–5574. [CrossRef]

15. Ohno, T.; Sarukawa, K.; Matsumura, M. Crystal faces of rutile and anatase TiO₂ particles and their roles in photocatalytic reactions. *New J. Chem.* **2002**, *26*, 1167–1170. [[CrossRef](#)]
16. Zhang, L.; Wang, W.; Sun, S.; Jiang, D.; Gao, E. Selective transport of electron and hole among {0 0 1} and {1 1 0} facets of BiOCl for pure water splitting. *Appl. Catal. B Environ.* **2015**, *162*, 470–474. [[CrossRef](#)]
17. Kaur, J.; Singh, J.; Rawat, M. An efficient and blistering reduction of 4-nitrophenol by green synthesized silver nanoparticles. *SN Appl. Sci.* **2019**, *1*, 1060. [[CrossRef](#)]
18. Verdine, J.C. Metal oxides in heterogeneous oxidation catalysis: State of the art and challenges for a more sustainable world. *ChemSusChem* **2019**, *12*, 577–588.
19. Alam, M.W. Electrochemical Sensing of Dextrose and Photocatalytic Activities by Nickel Ferrite Nanoparticles Synthesized by Probe Sonication Method. *Curr. Nanosci.* **2021**, *17*. [[CrossRef](#)]
20. Khan, M.S.; Ashiq, M.N.; Ehsan, M.F.; He, T.; Ijaz, S. Controlled synthesis of cobalt telluride superstructures for the visible light photo-conversion of carbon dioxide into methane. *Appl. Catal. A Gen.* **2014**, *487*, 202–209. [[CrossRef](#)]
21. Alam, M.W.; Rao, T.N.; Prashanthi, Y.; Sridhar, V.; Alshoabi, A.; Souayeh, B.; Abuhimd, H.; Ahmed, F. Application of Silica Nanoparticles in the Determination of Herbicides in Environmental Water Samples Using Liquid Chromatography-Mass Spectroscopy. *Curr. Nanosci.* **2020**, *16*, 748–756. [[CrossRef](#)]
22. Fujishima, A.; Hashimoto, K.; Watanabe, T. *TiO₂ Photocatalysis Fundamentals and Applications, A Revolution in Cleaning*; BKC: Tokyo, Japan, 1999.
23. Fujishima, A.; Honda, K. Photolysis-decomposition of water at the surface of an irradiated semiconductor. *Nature* **1972**, *238*, 37–38. [[CrossRef](#)]
24. Muthee, D.K.; Dejene, B.F. Effect of annealing temperature on structural, optical and photocatalytic properties of titanium dioxide nanoparticles. *Heliyon* **2021**, *7*, e07269. [[CrossRef](#)] [[PubMed](#)]
25. Chaturvedi, S.; Dave, P.N.; Shah, N. Applications of nano-catalyst in new era. *J. Saudi Chem. Soc.* **2012**, *16*, 307–325. [[CrossRef](#)]
26. Ziental, D.; Czarczynska-Goslinska, B.; Mlynarczyk, D.T.; Glowacka-Sobotta, A.; Stanisz, B.; Goslinski, T.; Sobotta, L. Titanium dioxide nanoparticles: Prospects and applications in medicine. *Nanomaterials* **2020**, *10*, 387. [[CrossRef](#)] [[PubMed](#)]
27. Mahshid, S.; Askari, M.; Ghamsari, M.S. Synthesis of TiO₂ nanoparticles by hydrolysis and peptization of titanium iso-propoxide solution. *J. Mater. Process. Technol.* **2007**, *189*, 296–300. [[CrossRef](#)]
28. O'regan, B.; Gratzel, M. A low cost, high efficiency solar cell based on dye sensitized colloidal TiO₂ films. *Nature* **1991**, *353*, 737–740. [[CrossRef](#)]
29. Eidsvåg, H.; Bentouba, S.; Vajeeston, P.; Yohi, S.; Velauthapillai, D. TiO₂ as a Photocatalyst for Water Splitting—An Experimental and Theoretical Review. *Molecules* **2021**, *26*, 1687. [[CrossRef](#)]
30. Li, G.; Richter, C.P.; Milot, R.L.; Cai, L.; Schmuttenmaer, C.A.; Crabtree, R.H.; Brudvig, G.W.; Batista, V.S. Synergistic effect between anatase and rutile TiO₂ nanoparticles in dye-sensitized solar cells. *Dalton Trans.* **2009**, 10078–10085. [[CrossRef](#)]
31. Ahn, W.-Y.; Sheeley, S.A.; Rajh, T.; Cropek, D.M. Photocatalytic reduction of 4-nitrophenol with arginine-modified titanium dioxide nanoparticles. *Appl. Catal. B Environ.* **2007**, *74*, 103–110. [[CrossRef](#)]
32. Ni, M.; Leung, M.K.; Leung, D.Y.C.; Sumathy, K. A review and recent development in photocatalytic water-splitting using TiO₂ for hydrogen production. *Renew. Sustain. Energy Rev.* **2007**, *11*, 401–425. [[CrossRef](#)]
33. Han, F.; Kambala, V.S.R.; Srinivasan, M.; Rajarathnam, D.; Naidu, R. Tailored titanium dioxide photocatalysts for the degradation of organic dyes in wastewater treatment: A review. *Appl. Catal. A Gen.* **2009**, *359*, 25–40. [[CrossRef](#)]
34. Liu, Z.; Wang, R.; Kan, F.; Jiang, F. Synthesis and Characterization of TiO₂ Nanoparticles. *Asian J. Chem.* **2014**, *26*, 655–659. [[CrossRef](#)]
35. Dubey, R.S.; Krishnamurthy, K.V.; Singh, S. Experimental studies of TiO₂ nanoparticles synthesized by sol-gel and sol-vothermal routes for DSSCs application. *Results Phys.* **2019**, *14*, 102390. [[CrossRef](#)]
36. Devi, R.; Venckatesh, R.; Sivaraj, R. Synthesis of Titanium Dioxide Nanoparticles by Sol-Gel Technique. *Int. J. Innov. Res. Sci. Eng. Technol.* **2014**, *3*, 15206–15211. [[CrossRef](#)]
37. Chu, L.; Qin, Z.; Yang, J.; Li, X. Anatase TiO₂ nanoparticles with exposed (001) facets for efficient dye-sensitized solar cells. *Sci. Rep.* **2015**, *5*, 12143–12152. [[CrossRef](#)]
38. Jule, L.T.; Ramaswamy, K.; Bekele, B.; Saka, A.; Nagaprasad, N. Experimental investigation on the impacts of annealing temperatures on titanium dioxide nanoparticles structure, size and optical properties synthesized through sol-gel methods. *Mater. Today Proc.* **2021**, *45*, 5752–5758. [[CrossRef](#)]
39. Babji, P.; Rao, I.N. Catalytic reduction of 4-nitrophenol by using Fe³⁺ and Ag⁺ Co-doped TiO₂ nanoparticles. *Int. J. Sci. Res.* **2015**, *4*, 2636–2641.
40. Vijayalaxmi, R.; Rajendran, V. Synthesis and characterization of nano TiO₂ via different methods. *Arch. Appl. Sci. Res.* **2012**, *4*, 1183–1190.
41. Soler-Illia, G.; Louis, A.; Sanchez, C. Synthesis and characterization of mesostructured titania-based materials through evaporation induced self assembly. *Chem. Mater.* **2002**, *14*, 750–759. [[CrossRef](#)]
42. Yu, J.C.; Zhang, L.; Zheng, A.Z.; Zhao, J. Synthesis and Characterization of Phosphated Mesoporous Titanium Dioxide with High Photocatalytic Activity. *Chem. Mater.* **2003**, *15*, 2280–2286. [[CrossRef](#)]
43. Kim, S.; Gupta, N.K.; Bae, J.; Kim, K.S. Fabrication of Coral-like Mn₂O₃/Fe₂O₃ nanocomposite for room temperature removal of hydrogen sulfide. *J. Environ. Chem. Eng.* **2021**, *9*, 105216. [[CrossRef](#)]

44. Bagheri, S.; Shameli, K.; Hamid, S.B.A. Synthesis and characterization of anatase titanium dioxide nanoparticles using egg white solution via sol-gel method. *J. Chem.* **2013**, *2013*, 848205. [[CrossRef](#)]
45. Jafri, N.M.; Jaafar, J.; Alias, N.; Samitsu, S.; Aziz, F.; Salleh, W.W.; Yusop, M.M.; Othman, M.; Rahman, M.; Ismail, A.; et al. Synthesis and Characterization of Titanium Dioxide Hollow Nanofiber for Photocatalytic Degradation of Methylene Blue Dye. *Membranes* **2021**, *11*, 581. [[CrossRef](#)]
46. Balcha, A.; Yadav, O.P.; Dey, T. Photocatalytic degradation of methylene blue dye by zinc oxide nanoparticles obtained from precipitation and sol-gel methods. *Environ. Sci. Pollut. Res.* **2016**, *23*, 25485–25493. [[CrossRef](#)] [[PubMed](#)]
47. Kundu, A.; Mondal, A. Photodegradation of methylene blue under direct sunbeams by synthesized anatase titania nanoparticles. *SN Appl. Sci.* **2019**, *1*, 280. [[CrossRef](#)]
48. Muthée, D.; Dejene, B. The effect of tetra isopropyl orthotitanate (TIP) concentration on structural, and luminescence properties of titanium dioxide nanoparticles prepared by sol-gel method. *Mater. Sci. Semicond. Process.* **2019**, *106*, 104783. [[CrossRef](#)]
49. Gupta, N.K.; Ghaffari, Y.; Bae, J.; Kim, K.S. Synthesis of coral-like α -Fe₂O₃ nanoparticles for dye degradation at neutral pH. *J. Mol. Liq.* **2020**, *301*, 112473. [[CrossRef](#)]
50. Ghaffari, Y.; Gupta, N.K.; Bae, J.; Kim, K.S. One-step fabrication of Fe₂O₃/Mn₂O₃ nanocomposite for rapid photodegradation of organic dyes at neutral pH. *J. Mol. Liq.* **2020**, *315*, 113691. [[CrossRef](#)]
51. Gupta, N.K.; Ghaffari, Y.; Kim, S.; Bae, J.; Kim, K.S.; Saifuddin, M. Photocatalytic degradation of organic pollutants over MFe₂O₄ (M = Co, Ni, Cu, Zn) nanoparticles at neutral pH. *Sci. Rep.* **2020**, *10*, 4942. [[CrossRef](#)]
52. Dagher, S.; Soliman, A.; Ziout, A.; Tit, N.; Hilal-Alnaqbi, A.; Khashan, S.A.; Alnaimat, F.; Qudeiri, J.E.A. Photocatalytic removal of methylene blue using titania–and silica-coated magnetic nanoparticles. *Mater. Res. Express* **2018**, *5*, 065518. [[CrossRef](#)]
53. Sarigul, G.; Chamorro-Mena, I.; Linares, N.; Garcia-Martinez, J.; Serrano, E. Hybrid amino acid–TiO₂ materials with tuneable crystalline structure and morphology for photocatalytic applications. *Adv. Sustain. Syst.* **2021**, *5*, 2100076. [[CrossRef](#)]
54. Devi, S.M.; Nivetha, A.; Prabha, I. Role of citric acid/glycine-reinforced nanometal oxide for the enhancement of physio-chemical specifications in catalytic properties. *J. Supercond. Nov. Magn.* **2020**, *33*, 3893–3901. [[CrossRef](#)]
55. Sanchez, U.A.; Chen, L.; Wang, J.A.; Norena, L.E.; Azomoza, M.; Solis, S.; Zhou, X.; Song, Y.; Liu, J. One-pot synthesis of W-TiO₂/SiO₂ catalysts for the photodegradation of p-Nitrophenol. *Int. J. Photoenergy* **2019**, *2019*, 13. [[CrossRef](#)]